Position Controller with Hysteresis Compensation for Magnetic Bearings *

Ralf Volkert, Oliver Radler,
Erik Weißenborn and Tom Ströhla

Dept. of Mechatronics
Technische Universität Ilmenau
P.O. Box 100565, 98684 Ilmenau, Germany
ralf.volkert@tu-ilmenau.de

Veit Zöppig

STZ Mechatronik
Ilmenau
Werner-von-Siemens-Str. 12, 98693 Ilmenau, Germany
veit.zoeppig@stz-mtr.de

***Abstract* – This paper deals with the Jiles-Atherton model for hysteresis effects and its inversion as well as its extension for the reproduction of force-current hysteresis loops. An identification procedure for the model parameters is presented for a given solenoid actuator. A simplified hysteresis compensation algorithm was implemented on a 16-bit Digital Signal Controller. The real-time hysteresis compensation quality both for constant and variable air gap lengths was first investigated by means of an open-loop force controller for a proportional solenoid. Finally a closed-loop position controller with hysteresis compensation for an electromagnet, which is part of a magnetic bearing system, is presented. Experimental results gained at the test rigs are shown and evaluated.**

***Index Terms* – Electromagnetic actuator, Jiles-Atherton hysteresis model, hysteresis compensation, position controller.**

I. Introduction

By combining electrodynamic drives with planar magnetic bearings, vacuum compatible integrated multi-coordinate drives with six degrees of freedom can reliably be realised, which are required for various modern applications, e.g. for the manufacture of integrated circuits. The demands on these new, more powerful and precise positioning systems grow year after year. Modern ultra-precision techniques require a positioning uncertainty below the 10 nm range with strokes of more than 200 mm in the *xy*-plane. The magnetic bearings used in these drives usually consist of several reluctance actuators. Besides the non-linearities due to magnetic saturation effects and eddy currents the control performance is influenced by the magnetic hysteresis. To attain a linear force-current relation and thus to improve the control performance compared to a simple PID controller, a more precise modelling of non-linearities and disturbing influences is necessary as well as a real-time compensation of the dominating magnetic hysteresis. Complex models are needed to describe this phenomenon with satisfying accuracy. The current state of the system depends on all former states.

There are several mathematical approaches for the accurate modelling of hysteresis effects. The hysteresis model describes, how the force F lags behind the evocative current I. This is a non-unique function $F(I)$. The implementation of the hysteresis compensation requests high CPU-intensity. It is also difficult to define the model parameters for different applications.

II. Hysteresis Model

A. The Jiles-Atherton Approach

The model developed by D.C. Jiles and D.L. Atherton for magnetic hysteresis belongs to the group of physical models, which take into account the actual physical processes inside a magnetic material [1] [2]. Movement and adhesion of magnetic domain borders near crystal defects cause a reversible magnetisation. An irreversible magnetisation arises from deformations of the domain borders. These effects are realised as variations from the anhysteretic curve. The Jiles-Atherton model offers a high accuracy and was mainly recommended for FEM calculations. Originally it is based on the Langevin model to calculate the magnetisation of paramagnetic materials. Langevin developed the relation between field strength H and magnetisation M with:

$$M = M_S \cdot \left(\coth\left(\frac{H}{a}\right) - \frac{a}{H} \right). \tag{1}$$

Thereby the parameter a is a material constant. The factor M_S (saturation magnetisation) arises for $H \to \infty$ and leads theoretically to a parallel orientation of all magnetic moments and to the applied field strength. For ferromagnetic materials Weiß introduced the "effective field" H_e. It is caused by the interaction of single domains, which generate an independent field $\overline{\alpha} \cdot M$, similar to a permanent magnet, due to the applied field strength and irreversible processes. The applied field strength and the independent field $\overline{\alpha} \cdot M$ result in the effective field strength:

$$H_e = H + \overline{\alpha} \cdot M \,. \tag{2}$$

* This work was funded by the German Research Foundation (DFG) within the Collaborative Research Centre 622 "Nanopositioning- and Nanomeasuring-Machines".

The factor $\overline{\alpha}$ represents a magnetic field parameter for the quantitative description of domain interactions. Equation (1) can be reshaped to calculate the anhysteretic magnetisation M_{an} for ferromagnetic materials:

$$M_{an} = M_S \cdot \left(\coth\left(\frac{H_e}{a} \right) - \frac{a}{H_e} \right), \tag{3}$$

$$M_{an} = M_S \cdot \left(\coth\left(\frac{H + \overline{\alpha} \cdot M}{a} \right) - \frac{a}{H + \overline{\alpha} \cdot M} \right). \tag{4}$$

To model the hysteresis of a material, Jiles and Atherton use a reversible part M_{rev} and an irreversible part M_{irr} for the magnetisation:

$$M = M_{rev} + M_{irr} . \tag{5}$$

For the irreversible part M_{irr} applies:

$$\frac{\mathrm{d}\, M_{irr}}{\mathrm{d}\, H} = \frac{M_{an}(H_e) - M_{irr}}{k \cdot \mathrm{sgn}\left(\frac{\mathrm{d}\, H}{\mathrm{d}\, t} \right) - \overline{\alpha} \cdot (M_{an}(H_e) - M_{irr})} . \tag{6}$$

The constant k is a degree for the energy losses per volume unit due to the resulting field M. By integration the irreversible component yields:

$$M_{irr} = \int \frac{\mathrm{d}\, M_{irr}}{\mathrm{d}\, H} \mathrm{d}\, H . \tag{7}$$

For the magnetisation M follows:

$$M = (1 - c) \cdot M_{irr} + c \cdot M_{an}(H_e) \tag{8}$$

with the reversibility coefficient c. From magnetisation M and field strength H the magnetic induction B is calculated:

$$B = \mu_0 \cdot (H + M) . \tag{9}$$

The magnetic B-H hysteresis is the reason for the force-current (F-I) hysteresis of electromagnets. Though, because of stray fields and inhomogeneities at the working air gap, the hystereses cannot be converted into each other. By means of a coordinate transformation (shifting, scaling) the F-I hysteresis can be mapped onto the point of origin. Then it acquires a shape similar to the one of the B-H hysteresis. The following experimentally gained transformation equations were applied:

$$H = c_H \cdot I \tag{10}$$

$$F = c_B \cdot B^2 \tag{11}$$

Due to the transformation, the F-I hysteresis is mapped onto the B-H hysteresis model. Therefore the five Jiles-Atherton model parameters a, M_S, $\overline{\alpha}$, k and c become abstract values, which cannot be assigned to certain characteristics of the F-I hysteresis loop. Yet to simplify matters, the original denotations were retained, although it is formally incorrect.

In [3] a method to invert the Jiles-Atherton model is introduced, which was originally intended for FEM simulations. The magnetic induction B is stated as an independent argument. Starting from the equations

$$\frac{\mathrm{d}\, M_{an}}{\mathrm{d}\, H_e} = \frac{M_S}{a} \cdot \left(1 - \coth^2\left(\frac{H_e}{a} \right) + \left(\frac{a}{H_e} \right)^2 \right) \tag{12}$$

and

$$\frac{\mathrm{d}\, M_{irr}}{\mathrm{d}\, B_e} = \frac{M_{an} - c \cdot M_{irr}}{\mu_0 \cdot k \cdot \mathrm{sgn}\left(\frac{\mathrm{d}\, H}{\mathrm{d}\, t} \right)} \tag{13}$$

with the saturation magnetisation M_S, the effective induction B_e and the material parameter a, the following differential equation is derived:

$$\frac{\mathrm{d}\, M}{\mathrm{d}\, B} = \frac{1 - c \cdot \frac{\mathrm{d}\, M_{irr}}{\mathrm{d}\, B_e} + \frac{c}{\mu_0} \cdot \frac{\mathrm{d}\, M_{an}}{\mathrm{d}\, H_e}}{1 + \mu_0 \cdot (1 - c) \cdot (1 - \overline{\alpha}) \cdot \frac{\mathrm{d}\, M_{irr}}{\mathrm{d}\, B_e} + c \cdot (1 - \overline{\alpha}) \cdot \frac{\mathrm{d}\, M_{an}}{\mathrm{d}\, H_e}} . \tag{14}$$

The magnetisation M is calculated by integrating (14). Together with the magnetic induction B the magnetic field strength H yields:

$$H = \frac{B}{\mu_0} - M . \tag{15}$$

Finally a coordinate transformation leads to an inverse model for the force-current hysteresis.

B. Identification of the Model Parameters

Exemplarily the F-I hysteresis loops of a solenoid actuator were measured for several air gap lengths (reference points) and currents. The applicability of the Jiles-Atherton model to describe the F-I hysteresis has to be proven. Therefore search algorithms are used to find suitable parameter sets for the five model parameters a, M_S, $\overline{\alpha}$, k, c and the two newly introduced scaling parameters c_H and c_B, which allow an exact reproduction of the measured hysteresis loops. This task can be converted into an optimisation problem with seven free parameters.

To define the quality of a parameter set, the sum of deviations between calculated and measured hysteresis curve at certain measuring points is determined (16). The optimisation algorithm tries to minimise this quality criterion.

$$Q_{JA} = \min\left[\sum_{j=1}^{j_{ges}} \left| F_{calc,j} - F_{meas,j} \right| \right], \tag{16}$$

where j_{ges} denotes the number of measuring points.

For higher accuracies also inner hysteresis loops are included in the parameter identification.

C. Optimisation Algorithms

In [4] some optimisation algorithms with regard to their applicability for this task are investigated. The possible solution space is first narrowed by an evolutionary optimisation algorithm according to Schwefel [5] in a very efficient way. Then for a more exact optimum localisation the well-known Nelder-Mead Simplex algorithm is executed starting with the parameter set found by the evolutionary search procedure.

Thus for every reference air gap an optimal parameter set was computed. In Fig. 1 the values found for the parameters k and c_H are marked with circles. Between these points spline interpolations were applied.

With the obtained parameter sets the measured *F-I* hystereses can be reproduced at the reference points in a highly accurate way. Yet, a parameter interpolation for air gap lengths between the measured reference points does not lead to physically reasonable results. The hysteresis loops calculated with interpolated parameters do not run between the loops evaluated for the adjoining reference points, but rather incoherent. Other optimisations with seven variable parameters show similar results.

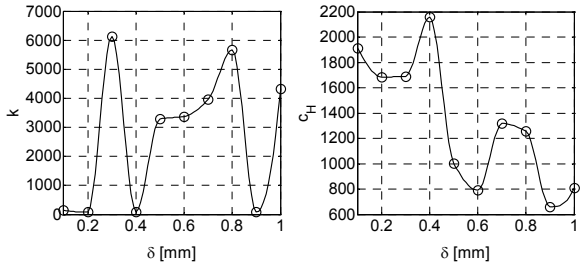

Fig. 1 Spline interpolated curves for the model parameters k and c_H, gained from optimisations.

It is known, that the force of the electromagnet continuously rises, if the air gap becomes smaller and the current remains constant. Therefore the hysteresis curve displayed in Fig. 2 for the air gap length $\delta = 0.45$ mm, which was calculated with interpolated parameters, cannot be correct.

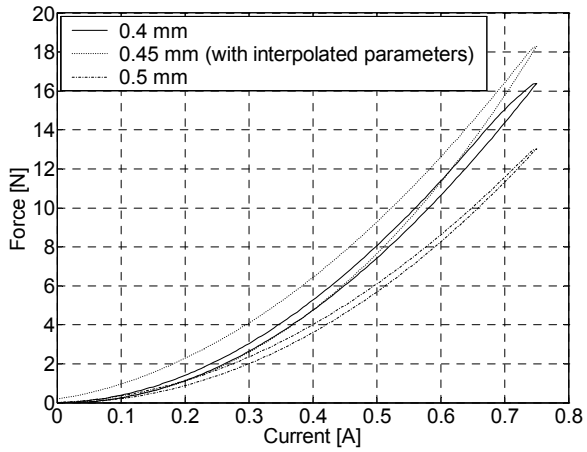

Fig. 2 Calculated hysteresis curves for different air gaps. Obviously the curve for $\delta = 0.45$ mm is not correct.

D. Reduction of the Number of Variable Parameters

For this reason the parameter optimisation procedure was modified to enable a realistic reproduction of the *F-I* hysteresis for every possible air gap length within the working range of the electromagnet. Thereby it was aspired, to keep constant as many parameters as possible, i.e., to reduce the number of variable parameters, which are necessary to calculate the hysteresis loops for different air gap lengths.

A proceeding with several optimisation cycles was successfully investigated. The computation of an optimal parameter set for a certain air gap length is performed by a combination of evolutionary and Simplex algorithm. After having calculated optimal parameter sets for all reference air gaps, one parameter is replaced by its average value. For the remaining variable parameters again optimal values are searched for all reference air gaps. This procedure is repeated, until only one variable parameter is left. For the optimisation sequence shown in Fig. 3 a MATLAB® program was developed, which automatically computes and saves the parameters needed for the hysteresis model.

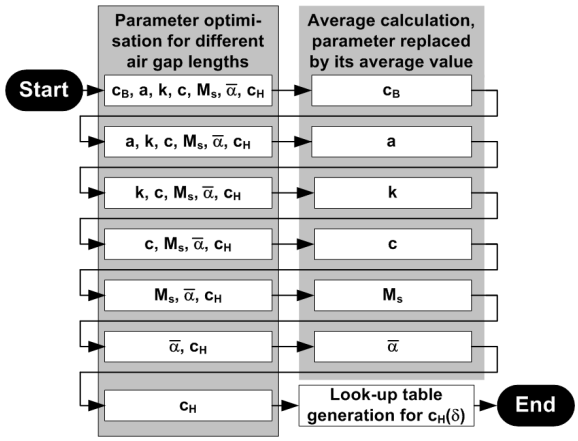

Fig. 3 Parameter optimisation sequence.

The best results were gained with c_H as the only variable parameter. For $c_H(\delta)$ (dependency of c_H on the air gap length δ) a continuous curve arises (Fig. 4).

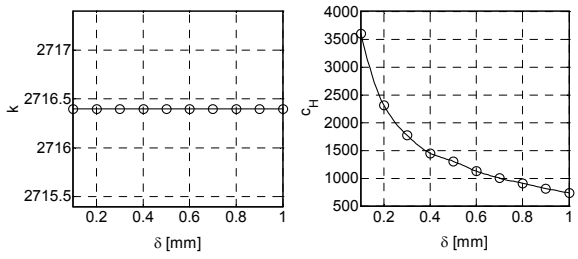

Fig. 4 Curves for the parameters k and c_H, gained from the modified optimisation sequence.

The usage of c_H as the only variable parameter implicates the advantage, that the Jiles-Atherton model can be computed with the same inner model parameters for all

air gap lengths. Subsequently the result is scaled through a multiplication by c_H (10).

To verify the results, again hysteresis loops for air gaps between the reference points were calculated. Now these hysteresis loops run exactly between those for the adjoining reference points, as shown Fig. 5. Thus the applicability of the identification procedure for the parameter of the *F-I* hysteresis model was proven.

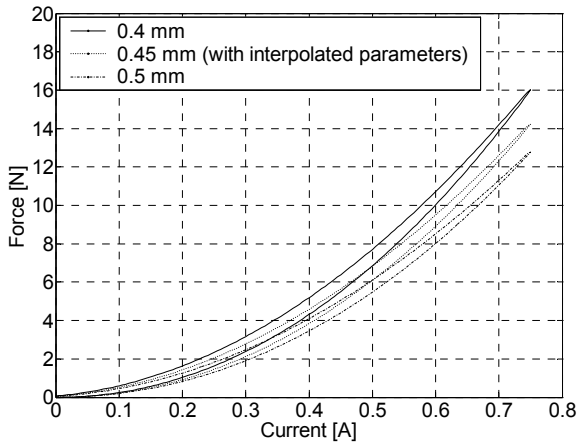

Fig. 5 Calculated hysteresis curves for different air gaps. The curve for $\delta = 0.45$ mm is correct.

III. Implementation of the Hysteresis Compensation on a Digital Signal Controller

A. Simplified Inverse Jiles-Atherton Model

The inverse Jiles-Atherton model allows a compensation of the electromagnet's force-current hysteresis. As it is based on the solution of a differential equation, it is suited for implementation on a digital signal processor. In this case the inverse Jiles-Atherton model was programmed for a Freescale 56F8322 16-bit Digital Signal Controller, which uses fixed-point arithmetic [6]. In order to apply the inverse Jiles-Atherton model for a real-time compensation, the adoption on the limitations of the fixed-point arithmetic is crucial.

The original model uses the hyperbolic cotangent (coth), which cannot be implemented directly. This affects the calculation of the anhysteretic magnetisation M_{an} and its derivative with respect to the effective field strength H_e:

$$M_{an} = M_S \cdot \left[\coth\left(\frac{H_e}{a}\right) - \frac{a}{H_e} \right], \tag{17}$$

$$\frac{\mathrm{d}M_{an}}{\mathrm{d}H_e} = \frac{M_s}{a} \cdot \left(1 - \coth^2\left(\frac{H_e}{a}\right) + \left(\frac{a}{H_e}\right)^2 \right). \tag{18}$$

It has been proven, that (17) can be approximated by a linear equation with sufficient accuracy. In the same way (18) can be approximated by a constant value:

$$M_{an} = K_2 + K_1 \cdot H_e, \tag{19}$$

$$\frac{\mathrm{d}M_{an}}{\mathrm{d}H_e} = K_1. \tag{20}$$

This simplified inverse Jiles-Atherton model was verified by simulation. The accuracy of the hysteresis compensation is not affected. Furthermore the approximation leads to a better stability and eliminates initial value problems.

B. Open-Loop Force Controller

The hysteresis compensation quality was then investigated at a proportional solenoid, which is used e.g. in oscillation isolation platforms. An LVDT sensor was applied for air gap measurement. The implemented open-loop force control, which provides a current depending on the desired force, leads to good succession behaviour both for constant and variable air gap lengths. Fig. 6 shows the hardware structure of the experimental set-up.

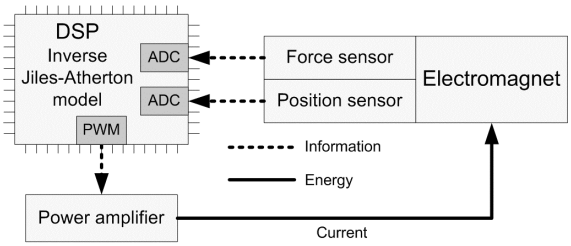

Fig. 6 Hardware structure.

The Jiles-Atherton model parameters were identified for the stroke end position and implemented in the controller program. A serial communication is used for sending the desired force values from the PC to the embedded controller. The desired force values and the measured force signals were recorded. The same desired force signal was used as input for a MATLAB® simulation of the controller program. In addition, the proportional solenoid was controlled without the hysteresis compensation. In this case it was assumed, that the actuator has a constant current-force ratio. Fig. 7 shows the experimental result.

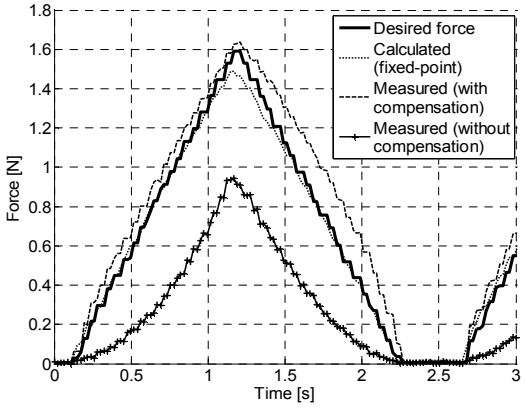

Fig. 7 Hysteresis compensation at a constant air gap.

The force signal measured with hysteresis compensation shows only small differences to the desired force curve and

the simulated one. In the next step the model parameters were adapted to the armature position in order to achieve a position-independent force control. For this purpose position-dependent look-up tables for the model parameters were used. The functioning of this approach was tested by measuring the force output for a triangular desired force signal for different discrete armature positions *x*. Fig. 8 shows the results of this experiment.

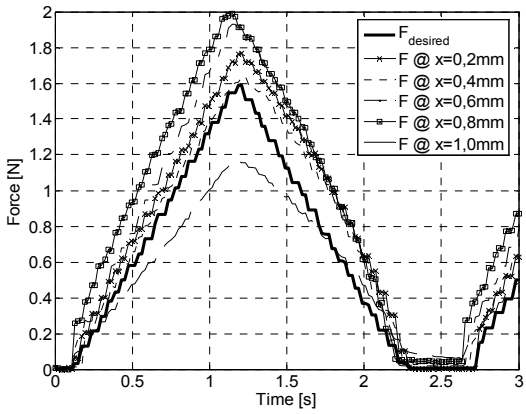

Fig. 8 Hysteresis compensation at different air gaps.

The triangular signal shape is achieved at every position of the armature's movement range. The force is controllable with a maximum relative error of 30 %. Without hysteresis compensation the signal shape differs strongly with respect to the desired triangular waveform.

IV. Position Controller with Hysteresis Compensation

A. Hardware-in-the-Loop Test Rig

To be able to test the hysteresis compensation algorithm in a closed-loop position controller, a hardware-in-the-loop test rig (Fig. 9) was built up. It includes an electromagnet, which was originally developed as part of a magnetic bearing system. Other important components of the test rig are the linear drive with the corresponding control electronics and a powerful modular real-time capable DSP system manufactured by dSPACE®.

The electromagnet is attached to the linear drive, which allows the simulation of a load for the electromagnet. Force and damping can be adjusted via a PC with LabView®. The linear drive's slider is guided by magnetically preloaded aerostatic bearings and driven by a moving coil actuator. Control is carried out via an analog power amplifier, whose current is set by the real-time data processing system ADwin GOLD® with an implemented state controller. The interpolated resolution of the incremental position measurement system is 50 nm. The controller for the distance between the electromagnet and the armature plate (position controller) is implemented in the dSPACE® system. This system consists of several hardware and software components, which allow operating the test rig, measuring and processing sensor signals in real-time as well as visualizing measured values.

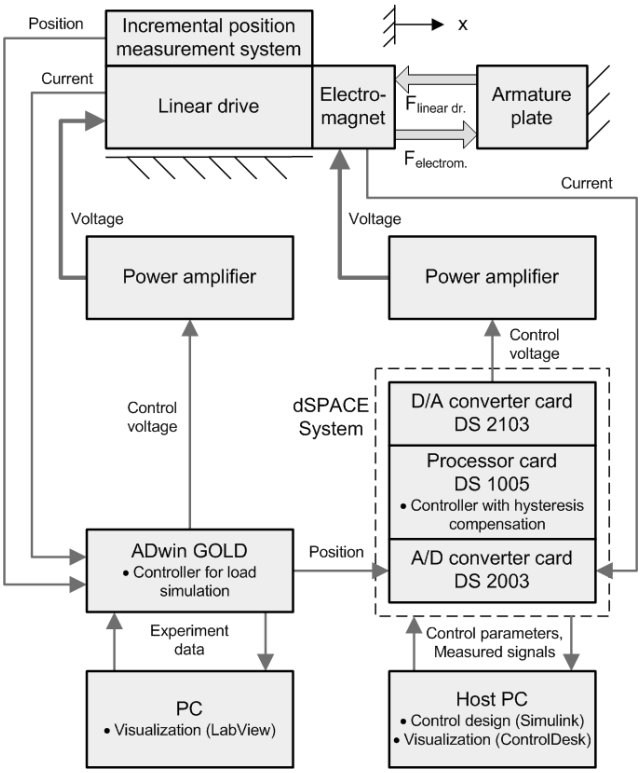

Fig. 9 Hardware-in-the-loop test rig.

MATLAB / Simulink® runs on the host PC, where the position controller is modelled. The model can be translated into program code suitable for the processor card without any further programming effort by means of a real-time-interface (RTI). A real-time control of the electromagnet is possible at once. The set value (control voltage) is generated by the D/A converter card DS 2103 and passed on from an analog power amplifier to the magnet coil. Sensor signals for position and current are transmitted to the processor card via the A/D converter card DS 2003. The software ControlDesk® offers a graphical user interface and allows constant monitoring of all system states and real-time tuning of control parameters.

B. Structure of the Position Controller

In the next step the design of a closed-loop position controller applying linear control techniques was taken into account. By using the inverse Jiles-Atherton model as part of the controller, the electromagnet's force-current hysteresis is compensated in real-time and an almost linear actuator behaviour is achieved.

At first the dynamic behaviour of the position controller with hysteresis compensation was simulated in MATLAB® together with an electromagnet model, which includes the dominating non-linearities [7]. The electrical subsystem with a look-up table containing the measured relation between flux linkage and current, the force-current hysteresis described with the Jiles-Atherton model, and the mechanical subsystem were implemented. A PID controller with an additional derivative part (PIDD^2

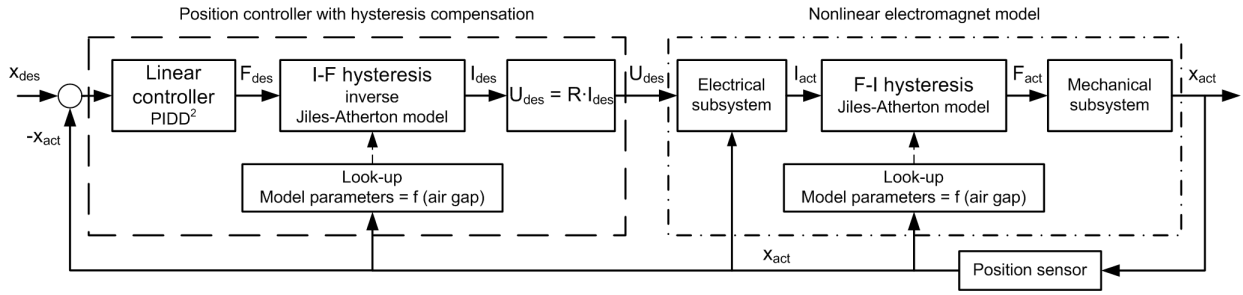

Fig. 10 Structure of the simulation model with hysteresis compensation.

controller) [7] in combination with the inverse Jiles-Atherton model was applied. Fig. 10 shows the structure of the simulation model containing the electromagnet and the position controller with hysteresis compensation.

Based on simulation results, the parameters of the PIDD^2 controller were manually adjusted at the real-time hardware-in-the-loop test rig (Fig. 9), where several step responses with different heights were measured. Alternatively a PIDD^2 controller without hysteresis compensation was investigated. Fig. 11 shows typical results.

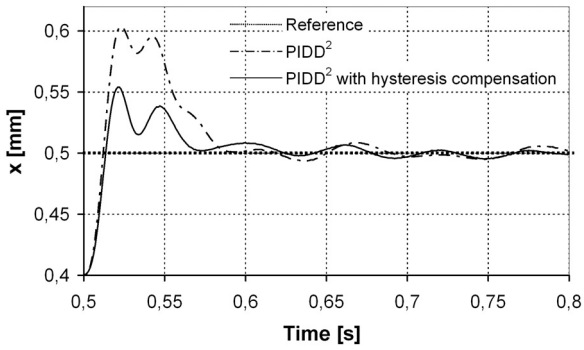

Fig. 11 Effect of the hysteresis compensation.

With hysteresis compensation an overshoot reduction of about 50 % was gained. Yet settling time and steady state error remain almost constant. An improvement of the PIDD^2 controller behaviour and a reduction of overshoot are expected from parameter optimisations in simulations or directly at the test rig.

V. Conclusion

The Jiles-Atherton model allows an effective and highly accurate description of hysteresis effects. By means of two different electromagnets it was exemplarily shown, that the Jiles-Atherton model, which was originally developed to describe the *B-H* hysteresis, can also be applied for the reproduction of the *F-I* hysteresis. Thus an extension of the model was performed. For the identification of the model parameters an algorithm was presented, which uses a combination of the evolutionary optimisation method according to Schwefel with the Nelder-Mead Simplex algorithm. The model parameters can be computed in a way, that only the scaling parameter c_H depends on the air gap length and the remaining parameters are constant.

A simplified inverse Jiles-Atherton model was programmed for a 16-bit Digital Signal Controller, which uses fixed-point arithmetic. With this hardware the real-time hysteresis compensation quality of the extended inverse Jiles-Atherton model was tested by means of an open-loop force control for a proportional solenoid, which is used e.g. in oscillation isolation platforms. The hysteresis compensation leads to a good control behaviour both for constant and variable air gap lengths.

In the next step a closed-loop position controller was tested both with and without the extended inverse Jiles-Atherton model. Therefore a hardware-in-the-loop test rig including an electromagnet, which was originally developed as part of a magnetic bearing system, was built up. Hysteresis acts as a disturbing influence limiting the control performance. Several step responses with different heights were measured at the test rig. With hysteresis compensation an overshoot reduction of up to 50 % is achievable.

As the position cannot be controlled more accurately than it is measured, laser interferometers or capacitance measuring systems will be used in future work steps to reach a higher resolution of 10 nm or less. Also the applicability of the hysteresis compensation by means of the inverse Jiles-Atherton model has to be proven for other actuator types, like e.g. piezoelectric or magnetostrictive actuators.

References

[1] D.C. Jiles and D.L. Atherton, "Theory of Ferromagnetic Hysteresis," *J. Magn. Magn. Mater.,* no. 61, pp. 48-60.

[2] A. Iványi, "Hysteresis Models in Electromagnetic Computation," Akadémiai Kiadó, Budapest, 1997.

[3] N. Sadowski, N.J. Batistela, J.P. Bastos and M. Lajoie-Mazenc, "An Inverse Jiles-Atherton Model to Take Into Account Hysteresis in Time-Stepping Finite-Element Calculations," *IEEE Trans. Magn.*, vol. 38, no. 2, pp. 797–800, March 2002.

[4] T. Ströhla and S. Bode, "Compensation of the Force Hysteresis of Proportional Solenoid Actuators," *Int. IEEE Conf. Mechatronics & Robotics*, Proc. vol. 2, pp. 442-445, Oct. 2004.

[5] H.P. Schwefel, „Numerische Optimierung von Computermodellen mittels der Evolutionsstrategien," Birkhäuser: Basel, Stuttgart, 1977.

[6] Freescale Semiconductor, "56F8322/56F8122 Data Sheet, Preliminary Technical Data," Rev.12.0, Freescale Semiconductor, 2005.

[7] R. Volkert, V. Kireev, J. Zentner and T. Bertram, "Nonlinear Control Design for the Magnetic Guidance of a Multi-Coordinate Positioning System," *ASPE Annual Meeting* (2005), Proc. pp. 202-205, Oct. 2005.